BioMetals 1995, **8**, 149–162

EPR and Mössbauer spectroscopic studies on the tetrameric, NAD-linked hydrogenase of *Nocardia opaca* 1b and its two dimers: 1. The $\beta\delta$-dimer—a prototype of a simple hydrogenase

Christiane Zaborosch*§, Michael Köster†, Eckhard Bill†, Klaus Schneider‡, Hans G. Schlegel* & Alfred X. Trautwein†

**Institut für Mikrobiologie der Universität Göttingen, †Institut für Physik der Medizinischen Universität zu Lübeck and ‡Lehrstuhl für Anorganische Chemie I der Universität Bielefeld, Germany*

Received 3 June 1994; accepted for publication 24 June 1994

The cytoplasmic, tetrameric NAD-linked hydrogenase from *Nocardia opaca* 1b can be separated in two dimeric substructures, an $\alpha\gamma$-dimer with NADH:electron acceptor oxidoreductase (diaphorase) activity and a $\beta\delta$-dimer which displays hydrogenase activity with artificial electron carriers. These two dimers were preparatively isolated by a FPLC Mono Q procedure in the absence of nickel and at alkaline pH values. The hydrogenase-active $\beta\delta$-dimer contained, as analyzed by inductively coupled plasma mass spectrometry (ICP-MS), 3.5–3.9 iron atoms and 1.3–1.7 nickel atoms per dimer molecule. EPR and Mössbauer spectra indicated the presence of a [4Fe-4S] cluster. This center turned out to be extremely labile towards oxidants. Oxidation led to irreversible convertion into a [3Fe-4S] form, thus representing an artifact and not a regulatory state of the cluster. The midpoint redox potential of the [4Fe-4S] cluster was determined to be −385 mV. Very weak EPR Ni signals of the $\beta\delta$-dimer were detectable in the oxidized as well as in the reduced state. The diaphorase-active $\alpha\gamma$-dimer was free of nickel and the iron content corresponded to 11.2–12.8 Fe atoms per dimer molecule. From EPR and Mössbauer measurements it was concluded that this dimer contained two [4Fe-4S] clusters, one [2Fe-2S] and one [3Fe-4S] cluster. In accordance with the results obtained for the dimer proteins, for the whole enzyme an iron content of 15.8–16.2 atoms per enzyme molecule have been determined. EPR spectra and spectrum simulations of the native hydrogenase corroborate the cluster assignments of the two dimers: in total the enzyme contains one [2Fe-2S] cluster, one [3Fe-4S] cluster and three [4Fe-4S] clusters.

Keywords: hydrogenase (or H_2:NAD^+ oxidoreductase, EC 1.12.1.2), *Nocardia opaca*, diaphorase-dimer, hydrogenase-dimer, EPR and Mössbauer spectroscopy.

Introduction

On the basis of the content of metal components hydrogenases can be divided into three main classes:

1 [Fe] hydrogenases containing only iron-sulfur clusters such as that isolated from *Desulfovibrio vulgaris* (Huynh *et al.* 1984), *Clostridium pasteurianum* (Adams & Mortenson 1984), *Megasphaera elsdenii* (Grande *et al.* 1983);
2 [NiFe] hydrogenases containing nickel and Fe-S clusters as the enzymes from diverse sulfate-reducing (*D. gigas*), photosynthetic (*Rhodobacter capsulatus*), methanogenic (*Methanobacterium thermoautotrophicum*) and hydrogen-oxidizing (*Alcaligenes eutrophus*) bacteria (Cammack *et al.* 1988);
3 [NiFeSe] hydrogenases containing Fe-S clusters and equimolar amounts of nickel and selenium as found in *D. baculatus* (Teixeira *et al.* 1987).

Two distinct types of [NiFe] hydrogenases exist in aerobic H_2-oxidizing bacteria, a cytoplasmic NAD-linked hydrogenase and a membrane-bound, respiratory chain-coupled enzyme. The best-investigated NAD-linked hydrogenases are the enzymes of *Alcaligenes eutrophus* H16 (Schneider & Schlegel 1976, Schneider *et al.* 1979, Schneider &

Address for correspondence: A. X. Trautwein, Institut für Physik der Medizinischen Universität zu Lübeck, Ratzeburger Allee 160, D-23538 Lübeck, Germany. Fax: (+49) 451 5004 214.
§Present address: Institut für Chemo- und Biosensorik, Münster, Germany.

Piechulla 1986) and *Nocardia opaca* 1b (Aggag & Schlegel 1974, Schneider *et al.* 1984a,b, Zaborosch *et al.* 1989). These two enzymes are tetramers consisting of four non-identical, serologically unrelated subunits (*N. opaca* M_r: α subunit 64000, β subunit 56000, γ subunit 31000, δ subunit 27000). *A. eutrophus* H16 contains in addition a membrane-bound hydrogenase which is composed of only two different subunits. This type of hydrogenase is present in the majority of aerobic hydrogen-activating bacteria and nitrogen-fixing bacteria (Lorenz *et al.* 1989).

It has been reported that the hydrogenase of *N. opaca* 1b, if prepared in the absence of Ni ions, can be cleaved into two dimeric proteins with different cofactor composition and different enzymatic activity (Schneider *et al.* 1984a,b). The nickel-containing $\beta\delta$-dimer shows H_2: acceptor oxidoreductase activity with several electron acceptors but not with NAD. This dimer must, therefore, contain the hydrogen activating center. The second, FMN-containing dimer consists of the α and γ subunit and is hydrogenase inactive. This protein shows diaphorase (NADH : acceptor oxidoreductase) activity.

In this work we developed a procedure for the separation and stabilization of the two dimers allowing spectroscopic studies (EPR, Mössbauer) of the individual proteins. The characterization of the redox components in the $\beta\delta$-dimer was of special interest, because it corresponds to a simple model of a hydrogenase.

Materials and methods

Materials

Diethylaminoethyl (DEAE)-Sephacel, phenyl-Sepharose, the FPLC apparatus and Mono Q HR 5/5 column were purchased from Pharmacia, Freiburg, Germany; acrylamide, sodium dodecylsulfate, urea, Serva Blue R, 2-hydroxy-1,4-naphthoquinone and anthraquinone-2-sulfonate from Serva Feinbiochemica, Heidelberg, Germany; methyl viologen, benzyl viologen, FAD and phenazine methosulfate from Sigma GmbH, Taufkirchen, Germany; indigotrisulfonate, indigocarmin, resorufin and safranin T from Aldrich, Steinheim, Germany and ^{57}Fe from Hempel, Düsseldorf, Germany. The sources of all other chemicals were as previously reported (Schneider & Schlegel 1976).

Organism and growth

N opaca 1b now classified as *Rhodococcus* sp. (DSM 427) was grown in a mineral medium (Schlegel *et al.* 1961) in the presence of 0.1% fructose under an atmosphere of 80% H_2, 10% O_2 and 10% CO_2 (Zaborosch *et al.* 1989). The harvested cells were washed as described previously (Schneider *et al.* 1984a) and stored at −20 °C.

Enzyme purification and enzyme assays

Hydrogenase was purified under aerobic conditions as described by Zaborosch *et al.* (1989). The enzyme activity of the native enzyme was measured at 30 °C by monitoring the reduction of NAD spectrophotometrically (Schneider *et al.* 1984a). H_2 uptake activity of the $\beta\delta$-dimer was assayed by measuring the reduction of methylene blue photometrically at 546 nm. The assay medium contained 50 mM H_2-saturated Tris-HCl buffer (pH 8.2) and 0.2 mM methylene blue. Before the reaction was started with the electron acceptor, the dimer was reductively activated by the addition of 50 μM dithionite. Diaphorase activity of the $\alpha\gamma$-dimer was measured with methylene blue as electron acceptor under analogous conditions providing NADH (0.6 mM) instead of H_2 as electron donor. The addition of dithionite was not required. The reaction rates were determined anaerobically under N_2. The protein concentration was estimated according to Beisenherz *et al.* (1953).

Isolation of dimers

The two dimers of the cytoplasmic hydrogenase from *N. opaca* 1b were separated and isolated by using a Mono Q ion-exchange column (HR 5/5) and a Pharmacia FPLC system. The column was equilibrated with 25 mM Tris-HCl buffer (pH 9.0). Native hydrogenase samples (2 mg purified protein in 0.2 ml per run) were applied to the column. The dimers were eluted with a discontinuous KCl gradient (56 ml, 0–1 M KCl) at a flow rate of 2 ml/min. Fractions of 1 ml were collected and tested for activity. The purity of the isolated dimers was confirmed by analytical SDS/polyacrylamide gel electrophoresis (PAGE) (Schneider & Piechulla 1986). Hydrogenase-active and diaphorase-active fractions were combined and concentrated separately.

Metal determination by inductively coupled plasma mass spectroscopy (ICP-MS)

The iron and nickel contents of six different native enzyme and dimer preparations were analyzed by ICP-MS with a VG Plasma Quad instrument (VG Elemental, Winsford, UK). For quantitative determinations HNO_3 (final concentration 0.65%) was added to each sample. Calibrations were performed with the isotopes, ^{56}Fe and ^{61}Ni in the range of 10–1000 p.p.b. As blank solution double-distilled water containing 0.65% HNO_3 was used. The experimental set up for the measurements was as described by Vanhoe *et al.* (1989).

Redox titration

Redox potential titrations with the $\beta\delta$-dimer were carried out in an apparatus similar to that described by Dutton (1978), with sodium dithionite as reductant under a flow of purified argon and in the presence of the following dye mediators: phenazine methosulfate, methylene blue, indogotrisulfate, indigocarmin, resorufin, safranin T, anthraquinone-2-sulfonate, 2-hydroxy-1,4-naphthoquinone, benzyl viologen and methyl viologen, all at a final concentration of 50 μM. The buffer used was 0.5 M MOPS, pH 7.0. The redox potential was measured with a combined platin/calomel electrode and a pH meter. The system was

calibrated against a quinhydrone standard. After equilibration for 1 min at 25 °C, EPR samples of ~ 180 µl were taken from the assay and frozen in liquid nitrogen. All potentials are quoted relative to the standard hydrogen electrode.

EPR spectroscopy

EPR spectra were recorded on an X-band spectrometer (Bruker ER 200D-SRC) which was equipped with standard rectangular cavity TE102, a helium flow cryostat (Oxford Instruments ESR 910) and a data acquisition system based on IBM PC (developed by us in Lübeck). The temperatures were measured with an Au(Fe)/Chromel thermocouple which is located just below the sample region. The sample temperature was calibrated by comparing the temperature dependence of a ferric low-spin signal (S = 1/2) with a Curie law-behaviour (Slappendel *et al.* 1980). Air-oxidized EPR samples were prepared by freezing ~ 180 µl of stock solution in a quartz tube (SQ 707, Spintec, Remshalden, Germany) in liquid nitrogen and stored for EPR measurements. Additional oxidations were performed by addition of 3 mM ferricyanide. Reduced samples were obtained under H_2 atmosphere by addition of 3 mM dithionite. After an equilibration time of 2 min under argon in the quartz tubes, the samples were frozen in liquid nitrogen for EPR measurements. In order to determine the ratio of the different cluster types, double integrations of the EPR signals which correspond to oxidized and reduced samples were carried out. The integrals were corrected for EPR-tube diameter and g value anisotropy (Aasa & Vänngård 1975). The g values of complex and overlapping spectra were obtained by computer simulation. The computer programme (Twilfer *et al.* 1981) calculates the absorption-derivative pattern for powder samples with effective spin S = 1/2, using microwave frequency, effective g values and line widths (Γ) as parameters. The line shapes of spin packets chosen were Gaussian. From the simulations g values could be determined with an overall accuracy of ± 0.003. Relative intensities are given throughout for non-saturating conditions.

Mössbauer spectroscopy

The Mössbauer spectrometer was of the constant-acceleration type, equipped with a source of 0.5–1.1 GBq ^{57}Co in rhodium matrix, a helium bath cryostat (MD 306, Oxford Instruments) and a superconducting magnet system (Oxford Instruments). To the tail of the bath cryostat a small field of 20 mT could be applied with the help of a permanent magnet. For the preparation of Mössbauer samples the enzyme had to be enriched in ^{57}Fe. Therefore *N. opaca* 1b was grown autotrophically in 10-l fermentors in the presence of 0.1% ^{57}Fe-citrate. Cells were harvested at the late logarithmic phase and washed as previously described (Schneider *et al.* 1984a). The native hydrogenase was purified (Zaborosch *et al.* 1989), and both dimers were isolated. The isolated dimer samples were concentrated to about 120 mg protein/ml. The material was then transferred to combined Mössbauer/EPR sample holders, frozen to 77 K and kept at this temperature until required. The sample holders were made of polyolefin tubes. The sample was filled in a tube of 3.5 mm × 3.5 mm cross-section and 15 mm length, i.e. a volume of ~ 180 µl. The outer dimension of the holder allowed us to mount it in the standard quartz dewar of the EPR 910 cryostat as well as in a Mössbauer bath cryostat. The Mössbauer γ-rays were transmitted perpendicular through lateral faces of 3.5 mm × 15 mm. Mössbauer spectra without magnetic splittings were analyzed by least-squares fits with Lorentzians. Spectra of diamagnetic compounds in strong applied fields were simulated using the nuclear Hamiltonian with mixed electric and magnetic interactions, spectra of paramagnetic compounds were simulated using the spin-Hamiltonian formalism (Trautwein *et al.* 1991). Isomer shifts are given with respect to α-Fe at room temperature.

Results

Isolation and stabilization of the two dimers

In previous studies (Schneider *et al.* 1984a,b) the separation of the tetrameric hydrogenase from *N. opaca* 1b into two distinct heterodimers ($\alpha\gamma$, $\beta\delta$) had been achieved by a preparative PAGE procedure in the absence of nickel ions in the buffer and at alkaline pH values. This method appeared to have the following disadvantages: (i) the yield of dimers was low (about 20%), (ii) the preparation time was relatively long, and (iii) contaminations of the samples by polyacrylamide components decreased the stability of the proteins and disturbed subsequent analyses and spectroscopic studies. These disadvantages were avoided by FPLC on a Mono Q column. A complete separation of both dimers was achieved when the column was equilibrated with an alkaline buffer of low ionic strength; 25 mM Tris-HCl, pH 9.0, turned out to be the optimal buffer. An important prerequisite for complete separation was the utilization of a discontinuous KCl gradient with concentrations as indicated in Figure 1. Under these conditions the $\alpha\gamma$-dimer (M_r: α subunit 64 000, γ subunit 31 000) was eluted at 320 mM KCl in the equilibration buffer and the $\beta\delta$-dimer (M_r: β subunit 56 000, δ subunit 27 000) was eluted between 380 and 400 mM KCl.

The $\alpha\gamma$-dimer preparation had a specific NADH: methylene blue oxidoreductase activity of 205 units/mg protein, while the $\beta\delta$-dimer preparation had a specific H_2: methylene blue oxidoreductase activity of 59 units/mg protein. Both separate dimers were inactive with NAD. This physiological acceptor was only reduced by the tetramer, the original holoenzyme, and, at a similar rate, also by the reconstituted protein. The yield of the isolated dimeric polypeptides was about 95% per run. The efficiency of the separation method was controlled by subsequent analytical SDS/PAGE (Figure 2) which demonstrated that both dimer preparations were homogeneous.

Because for the native enzyme tetramer the neutral pH region was optimal for stability, the previous dimer

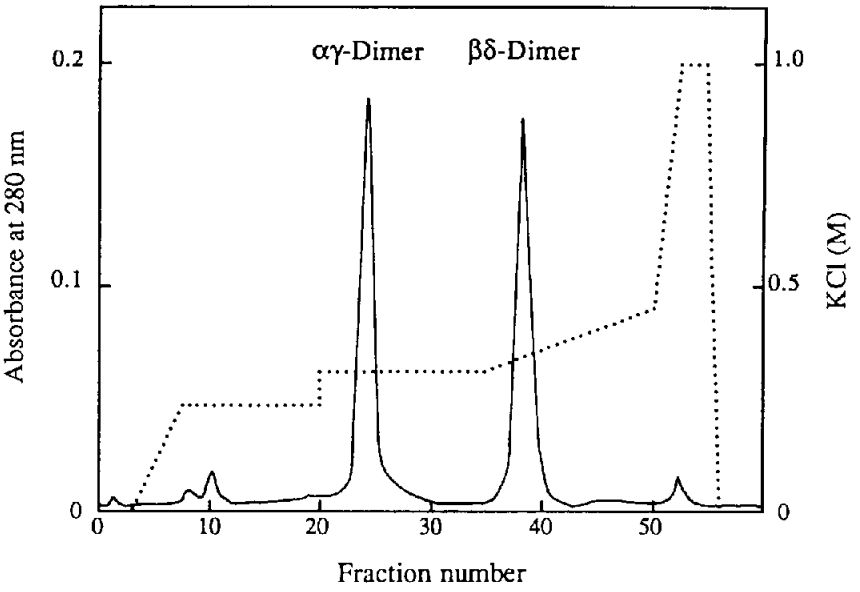

Figure 1. Separation of the two dimers of the hydrogenase from *N. opaca* 1b by FPLC on Mono Q HR 5/5.2 mg native hydrogenase was applied to the column (0.5 cm × 5 cm), the dimers were eluted with a discontinuous KCl gradient as indicated at a flow rate of 2 ml/min and fractions of 1 ml were collected. (– – –) protein; (· · · ·) KCl concentration.

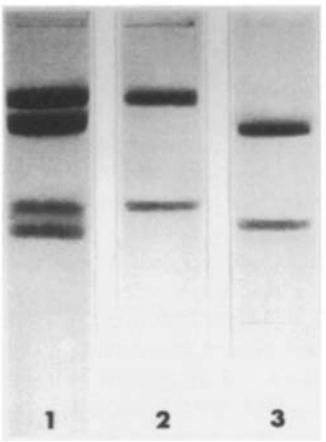

Figure 2. SDS/PAGE of the native hydrogenase and the two dimers from *N. opaca* 1b. The gel contained 7.5% acrylamide, 0.2% SDS, and 8 M urea and was run for 2 h at 80 mA and 200 V. Lane 1, whole enzyme (30 μg); lane 2, αγ-dimer (12 μg); lane 3, βδ-dimer (10 μg).

preparations were kept routinely at pH 7.0 after isolation. However, at this pH the βδ-dimer turned out to be very labile, losing more than 70% of the original activity overnight (at 4 °C under air). The optimal pH was in fact found to be 8.5 for the βδ-dimer, under these conditions no significant loss of activity was observed within several days, regardless of whether the atmosphere was air or H_2. The αγ-dimer did not exhibit a pronounced pH-dependent stability optimum, but a weakly alkaline pH (7.5–8.0) proved to be more appropriate than neutral pH.

Metal content

The content of iron and nickel in preparations of native hydrogenase and its dimers isolated from polyacrylamide gels, had previously been analyzed by energy dispersive X-ray fluorescence (Schneider *et al.* 1984b). These determinations yielded values of 12.4–14.7 iron atoms for the whole enzyme, based on an M_r of 178 000. By inductively coupled plasma mass spectrometry (ICP-MS) analyses, used in this work, we obtained a content of 15.8–16.2 iron atoms per enzyme molecule, based on the same M_r. The nickel content of the enzyme could not be determined definitely, because throughout the purification procedure all buffers contained 0.5 mM $NiCl_2$ to stabilize the hydrogenase. In previous work, Schneider *et al.* (1984b) determined 3.8 ± 0.1 nickel atoms per enzyme molecule in samples which were pre-treated with Chelex 100 to remove non-physiological nickel; despite this treatment the presence of nuisance nickel could not be prevented.

Metal analyses of the two dimers isolated by FPLC were performed by ICP-MS using six different preparations in each case. These determinations revealed that the αγ-dimer (M_r 95 000) contained 11.2–12.8 iron atoms per dimer molecule. This value is significantly higher than the value of 9.6 atoms per dimer molecule determined previously by the X-ray fluorescence method (Schneider *et al.* 1984b). In the αγ-dimer only trace concentrations of Ni of less than 0.1 mol/mol protein were found. The ICP-MS metal analyses indicated that, in accordance with X-ray fluorescence data, the βδ-dimer (M_r 83 000) contained 3.5–3.9 iron atoms and 1.3–1.7 nickel atoms per dimer molecule.

EPR spectra of the βδ-dimer

The βδ-dimer isolated by FPLC exhibited, in the dithionite-reduced state at 10 K, an EPR spectrum in the $g = 1.8–2.1$ region, representing a superposition of two signals, which could be clearly distinguished from each other by a different power saturation behaviour. One component (designated as H2) relaxed faster and dominated under saturating conditions (80 mW; Figure 3, spectrum a), whereas the other component (designated as H1) dominated under non-saturating conditions (0.2 mW; Figure 3, spectrum b). This low-power spectrum could be simulated by the superimposition of two signals (Figure 3,

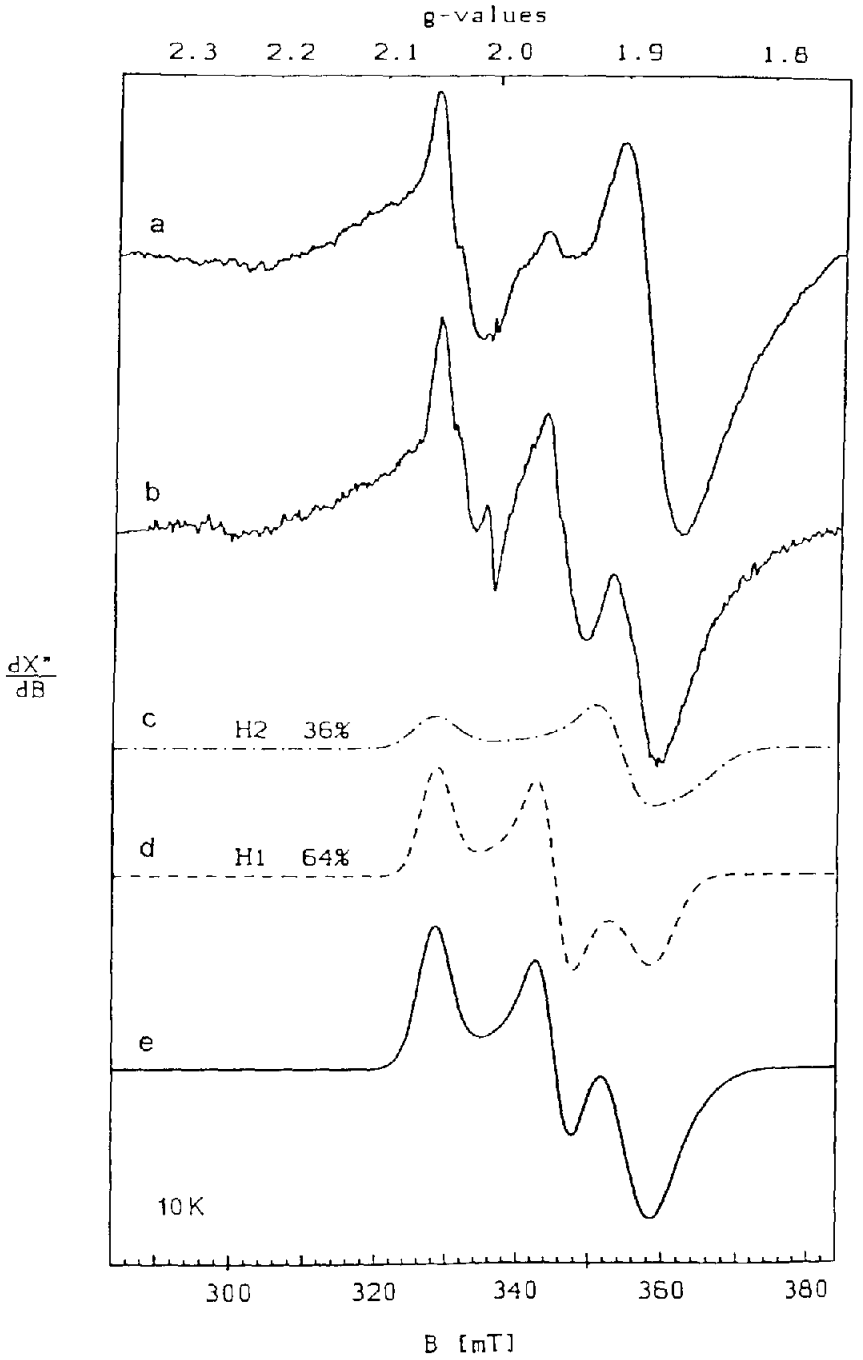

Figure 3. Experimental and simulated EPR spectra of $\beta\delta$-dimer preparations. $\beta\delta$-dimer (11 mg/ml) reduced with 3 mM dithionite recorded at 10 K, modulation amplitude 1 mT, (**a**) microwave power 80 mW; (**b**) microwave power 0.2 mW. frequency 9.417 GHz; (**c**) H2: g = 2.050, 1.898, 1.854 and Γ = 3.5, 3.0, 5.0 mT; (**d**) H1: g = 2.048, 1.948, 1.875 and Γ = 2.5, 2.8, 2.5 mT; (**e**) 64:36 superposition of simulated subspectra H1 : H2.

spectrum e), the signal of component H1 at g = 2.048, 1.948, 1.875 and the signal of component H2 at g = 2.050, 1.898, 1.854 (Figure 3, simulated spectra c and d). The proportion of component H1 in this spectrum was 64%, that of component H2 was 36%. Both signals are typical for $[4Fe\text{-}4S]^{1+}$ clusters. However, there are several lines of evidence that the two signals described do not arise from two different $[4Fe\text{-}4S]^{1+}$ clusters, but rather from one such cluster in two different protein conformations. Firstly the intensity ratio of the two signals varied from preparation to preparation: the more the signal of H1 was predominant, the higher was the activity. We therefore associated H1 with the intact, normally active enzyme, and H2 rather with an inactive/less active enzyme form. Secondly, this view is consistent with the fact that the signal of H1, but not that of H2, could be detected in the native enzyme tetramer. Finally, even the most active $\beta\delta$-dimer preparation did not contain more than four Fe atoms.

The midpoint redox potential of the [4Fe-4S] cluster was determined to be −385 mV, and it was found to be identical for both H1 and H2. Increase of the EPR signal intensity correlated well with the increase of the enzyme activity followed during the redox titration (data not shown). Maximum activity was reached at −420 mV.

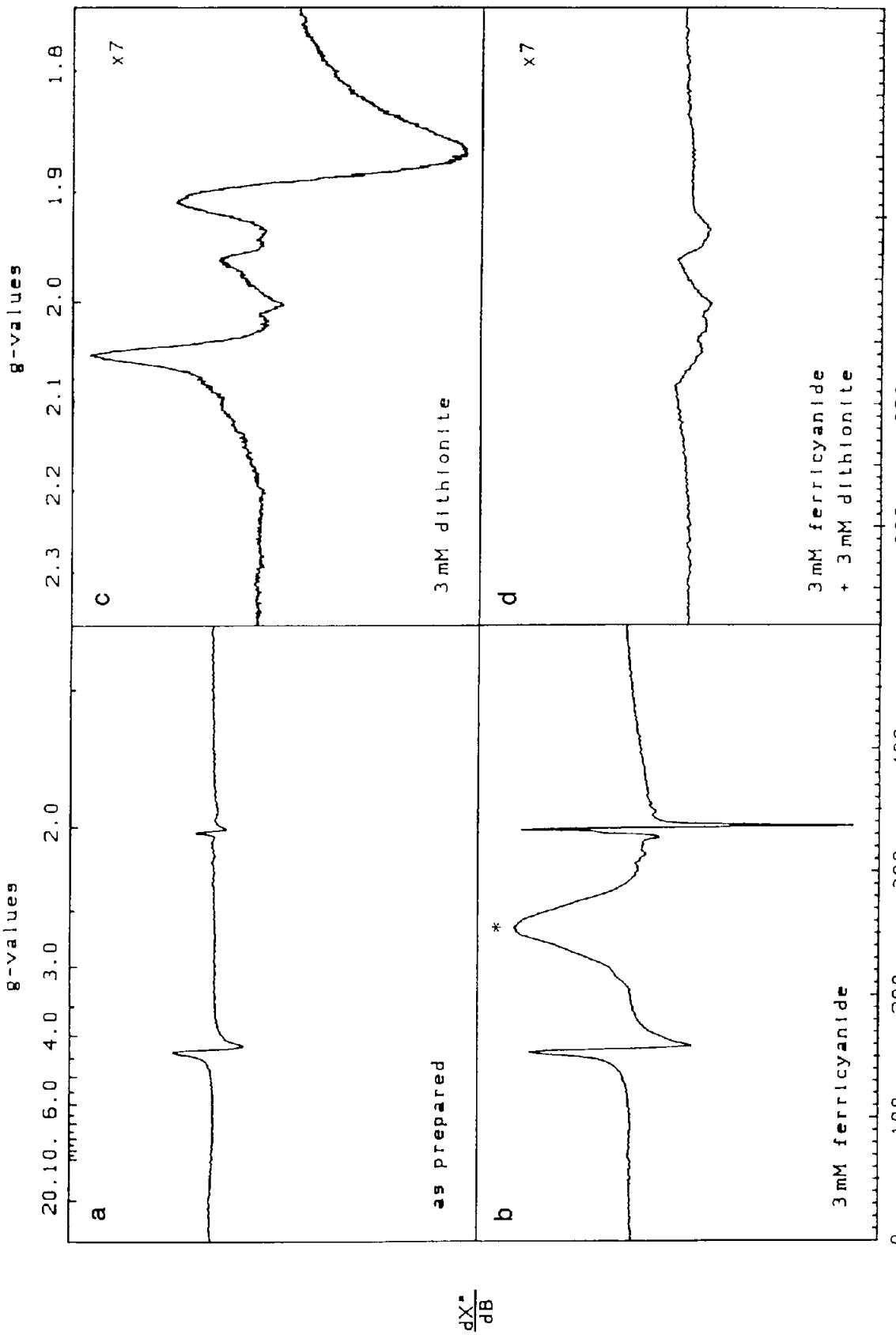

Figure 4. Effect of ferricyanide treatment on EPR spectra of $\beta\delta$-dimer preparations. Dimer samples (11 mg/ml) in the oxidized (**a**, **b**) and the dithionite-reduced state (**c**, **d**); samples before (**a**, **c**) and after (**b**, **d**) incubation with 3 mM ferricyanide. All spectra were measured at 10 K, modulation amplitude 1 mT, frequency 9.419 GHz, microwave power 2.0 mW (**a**, **b**) or 20 mW (**c**, **d**). Spectra (**c**) and (**d**) were enlarged 7-fold. The strong line at $g \approx 2.8$ in (**b**) marked by * is a low-spin ferric signal from ferricyanide.

The $\beta\delta$-dimer in the air-oxidized 'as prepared' state showed only a weak signal at $g = 2.02$ characteristic of $[3Fe\text{-}4S]^{+1}$ clusters (Figure 4a). The signal intensity corresponded to less than 4% compared with the EPR signals of the $[4Fe\text{-}4S]^{+1}$ cluster (Figure 4c). In addition, oxidized samples always exhibited a signal at $g = 4.3$, characteristic of monomeric (non-functional), high-spin ferric ions. Its intensity was preparation-dependent and was, as shown in Figure 4a, approximately 10 times greater than that of the $[3Fe\text{-}4S]^{+1}$ signal (assuming equal thermal population of the three Kramers' doublets of monomeric iron S = 5/2 at 10 K).

In order to elucidate the question concerning the nature of the [3Fe-4S] cluster, we assessed the influence of an oxidative treatment on the [4Fe-4S] cluster. EPR samples of the $\beta\delta$-dimer were incubated with ferricyanide and the comparison of the EPR spectra of untreated (Figure 4a) and ferricyanide-treated samples (Figure 4b) showed that the oxidation caused a strong increase of both the $[3Fe\text{-}4S]^{+1}$ signal and the signal at $g = 4.3$. Rereduction of the enzyme with dithionite resulted in a spectrum (Figure 4d) which was found to be strongly attenuated compared with that (Figure 4c) obtained after the first reduction of the 'as prepared' sample. Similar but less drastic effects were observed for $\beta\delta$-dimer samples after oxygen-treatment. The results demonstrate that the [4Fe-4S] cluster can be converted to a [3Fe-4S] cluster by oxidants, due to the loss of an iron atom, and that the original [4Fe-4S] cluster cannot be restored by reduction.

Attempts to reconvert the [3Fe-4S] to the [4Fe-4S] cluster by incubation of $\beta\delta$-dimer samples under reducing conditions in the presence of Fe(II) and dithiothreitol also failed in contrast to experiments performed with aconitase and ferredoxin II isolated from *Desulfovibrio gigas* (Moura *et al.* 1982, 1984). Activity measurements of ferricyanide-treated samples proved that the formation of the [3Fe-4S] cluster and the dimer inactivation are correlated. Both processes, [3Fe-4S] formation and inactivation, were dependent on the ferricyanide concentration and on the incubation time and were shown not to be reversible. Summarizing these results, we conclude that the [3Fe-4S] cluster, present in $\beta\delta$-dimer preparations, is not a natural constituent but an artifact resulting from an oxidative damage of the [4Fe-4S] cluster.

Weak Ni signals were only detectable if very high protein concentrations were used (not shown). This was the case with both the $\beta\delta$-dimer and the native tetrameric hydrogenase. The reason for the absence of a relevant Ni signal in the oxidized protein might be that Ni in this type of hydrogenase is, in spite of aerobic preparation, predominantly present in the EPR-silent '2+' oxidation state. Dithionite-reduced dimer samples were, with regard to Ni, already 'over-reduced'. In the course of the redox titration, performed with the $\beta\delta$-dimer, a transient Ni signal appeared and disappeared in a region between −300 and −380 mV. The protein solution used in this titration was rather dilute, and thus the Ni signals were too weak for quantitative evaluation.

Mössbauer spectra of the βδ-dimer

Mössbauer measurements with the EPR sample of oxidized $\beta\delta$-dimer were performed at 4.2 K in fields of 20 mT and 4.13 T. Two quadrupole doublets without magnetic splitting appeared in the 20 mT spectrum which is shown in Figure 5. Least-squares fits with Lorentzians revealed the following parameters: subspectrum 1, isomer shift $\delta =$ 0.42 mm/s, quadrupole splitting $\Delta E_Q = 1.27$ mm/s, line width $\Gamma = 0.33$ mm/s, 67.7% of total absorption area; subspectrum 2, $\delta = 0.23$ mm/s, $\Delta E_Q = 0.58$ mm/s, $\Gamma =$ 0.45 mm/s, 32.3% of total absorption area. Isomer shift and quadrupole splitting of the major component, subspectrum 1, are in agreement with those found for iron of the formal valence '2.5+' in oxidized $[4Fe\text{-}4S]^{2+}$ clusters

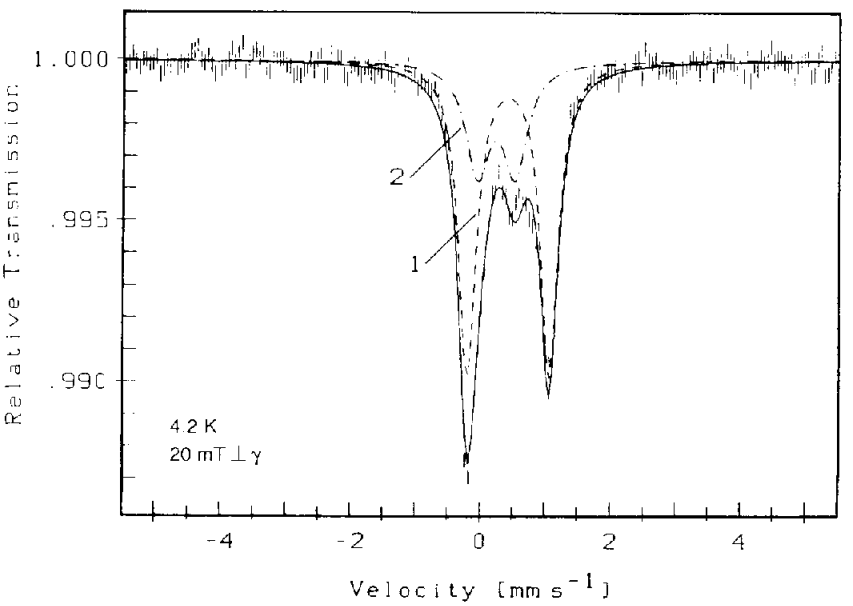

Figure 5. Mössbauer spectra of the oxidized $\beta\delta$-dimer, recorded at 4.2 K in a field of 20 mT, applied perpendicular to the γ-rays. The subspectra (– – – and – · –) are fits with Lorentzian lines.

(Middleton *et al.* 1980), while low isomer shift of subspectrum 2 indicates ferric ions in tetrahedral sulfur coordination (Orme-Johnson & Orme-Johnson 1982). An assignment of component 2 to $[3Fe\text{-}4S]^{1+}$ clusters, which contain only ferric high-spin iron (Emptage *et al.* 1980, Münck 1982), corroborates the EPR finding of preparation-dependent amounts of $[3Fe\text{-}4S]^{1+}$ clusters present in oxidized samples. Thus, the Mössbauer results obtained from oxidized $\beta\delta$-dimers are in qualitative agreement with the EPR results.

EPR spectra of the $\alpha\gamma$-dimer

The previously published EPR spectrum of the oxidized diaphorase-active $\alpha\gamma$-dimer isolated by PAGE had shown a relatively weak and broad signal at $g = 2.008$ (Schneider *et al.* 1984b). In contrast, the $\alpha\gamma$-dimer samples now prepared by FPLC showed a strong signal with narrow lines in the oxidized state (Figure 6a). Simulation of this spectrum gave g values of 2.018, 2.002, 1.985 which are typical for $[3Fe\text{-}4S]^{1+}$ clusters but deviate significantly from the g values of the $[3Fe\text{-}4S]^{1+}$ cluster artefact in the oxidized $\beta\delta$-dimer.

In the dithionite-reduced state the $\alpha\gamma$-dimer yielded a complex EPR spectrum at 10 K as shown in Figure 6b. Since the reduced three-iron cluster $[3Fe\text{-}4S]^{0}$ has system spin S = 2 (Thomson *et al.* 1981) and is therefore EPR-silent, the EPR spectrum reflects other iron clusters. By simulations we were able to decompose the spectrum in three components, i.e. D2, D4a and D4b. The superposition of these subspectra (solid line) revealed relative integral intensities of 33.3% for each. The three components exhibited very different temperature dependences. At 80 K the components D4a and D4b were strongly attenuated by relaxation broadening, and component D2 dominated the spectrum (Figure 6c). From a comparison of g values and temperature dependences of the components D2, D4a and D4b with published data (Rupp *et al.* 1978), we correlate D4a and D4b with $[4Fe\text{-}4S]^{1+}$ clusters and D2 with a $[2Fe\text{-}2S]^{1+}$ cluster.

In summary, the ratio of the integral intensity of the $[3Fe\text{-}4S]^{1+}$ spectrum from oxidized $\alpha\gamma$-dimers (Figure 6a) to the integral intensity of the components D2, D4a and D4b in reduced $\alpha\gamma$-dimers (Figure 6b) is 1 : 2.9. From our relative assignments in conjunction with the absolute metal content of 11.2–12.8 iron atoms per $\alpha\gamma$-dimer, we conclude that each $\alpha\gamma$-dimer contains two [4Fe-4S] clusters, one [3Fe-4S] and one [2Fe-4S] cluster.

The postulate that the [3Fe-4S] cluster is a physiological constituent of the $\alpha\gamma$-dimer was supported by oxidation experiments with ferricyanide. In contrast to the $\beta\delta$-dimer, the oxidative treatment (with 3 mM ferricyanide) of the $\alpha\gamma$-dimer did neither cause a significant enhancement of the $[3Fe\text{-}4S]^{1+}$ signal, nor did it induce any formation of ferric ions (with $g = 4.3$). In accordance with this spectroscopic observation, the ferricyanide treatment did not significantly affect the specific activity of the $\alpha\gamma$-dimer.

Mössbauer spectra of the $\alpha\gamma$-dimer

A Mössbauer spectrum of the air-oxidized $\alpha\gamma$-dimer was recorded at 4.2 K in a field of 20 mT applied perpendicular to the γ-rays (Figure 7a). The spectrum consists of two quadrupole doublets without apparent magnetic splittings. Isomer shifts and quadrupole splittings were determined from least-squares fits with Lorentzians: subspectrum 1, $\delta = 0.45$ mm/s, $\Delta E_Q = 1.21$ mm/s, $\Gamma = 0.4$ mm/s, 61% of total absorption area; subspectrum 2, $\delta = 0.35$ mm/s, $\Delta E_Q = 0.61$ mm/s, $\Gamma = 0.37$ mm/s, 39% of total absorption area. The parameters of subspectrum 1 are characteristic of $[4Fe\text{-}4S]^{2+}$ clusters (Middleton *et al.* 1980), as mentioned above for the $\beta\delta$-dimer, while those of subspectrum 2 are consistent with parameters of $[3Fe\text{-}4S]^{1+}$ clusters (Münck 1982, Orme-Johnson & Orme-Johnson 1982) and $[2Fe\text{-}2S]^{2+}$ clusters (Dunham *et al.* 1971). The relative intensities of subspectra 1 and 2, 61% and 39% of the total absorption area, are in agreement with the values 61.5% and 38.5%, expected for two [4Fe-4S] clusters, accounting for subspectrum 1 as well as one [3Fe-4S] and one [2Fe-2S] cluster accounting for subspectrum 2.

These assignments could be corroborated by the analysis of a magnetically perturbed Mössbauer spectrum. The experimental spectrum of an oxidized $\alpha\gamma$-dimer recorded at 4.2 K with an applied field of 4.13 T (Figure 7b) is dominated by the strong diamagnetic contributions of the $[4Fe\text{-}4S]^{2+}$ clusters (subspectrum 1, 61.5%) and the $[2Fe\text{-}2S]^{2+}$ clusters (subspectrum 2a, 15.4%). No indications are detectable for a subspectrum with wide magnetic splitting originating from paramagnetic $[3Fe\text{-}4S]^{1+}$ clusters with slow spin relaxation, as observed for hydrogenase from *Desulfovibrio gigas* (Teixeira *et al.* 1989). However, a simulation adopting fast spin relaxation with the typical spin-Hamiltonian parameters for a $[3Fe\text{-}4S]^{1+}$ cluster (Teixeira *et al.* 1989; subspectrum 2b, 23.1%) is consistent with the experimental data. Hence, also the high-field Mössbauer data indicate, that the $\alpha\gamma$-dimer contains two [4Fe-4S] clusters, one [3Fe-4S] and one [2Fe-2S] cluster.

EPR spectra of the native hydrogenase

The purified *N. opaca* hydrogenase tetramer in its oxidized state, as prepared under aerobic conditions, showed an EPR spectrum at 10 K (Figure 8a) with a prominent resonance at g=2.02 which is typical for $[3Fe\text{-}4S]^{1+}$ clusters, and a broad feature at $g = 1.95$, which probably results from magnetic interactions of the [3Fe-4S] cluster in the $\alpha\gamma$-dimer with a close paramagnetic site. A possible candidate for such a site is Ni^{2+} (S = 1, EPR-silent; More *et al.* 1986), although the Ni center is located in the other dimer. The suggestion that a spin coupling exists between two redox components located in different subunits is supported by the fact that the occurrence of the 1.95 resonance was observed only with the native or reconstituted tetramer (compare Schneider *et al.* 1984b) but with none of the separated dimers.

Reduction of the native hydrogenase tetramer of *N. opaca* with dithionite led to a complex EPR spectrum at

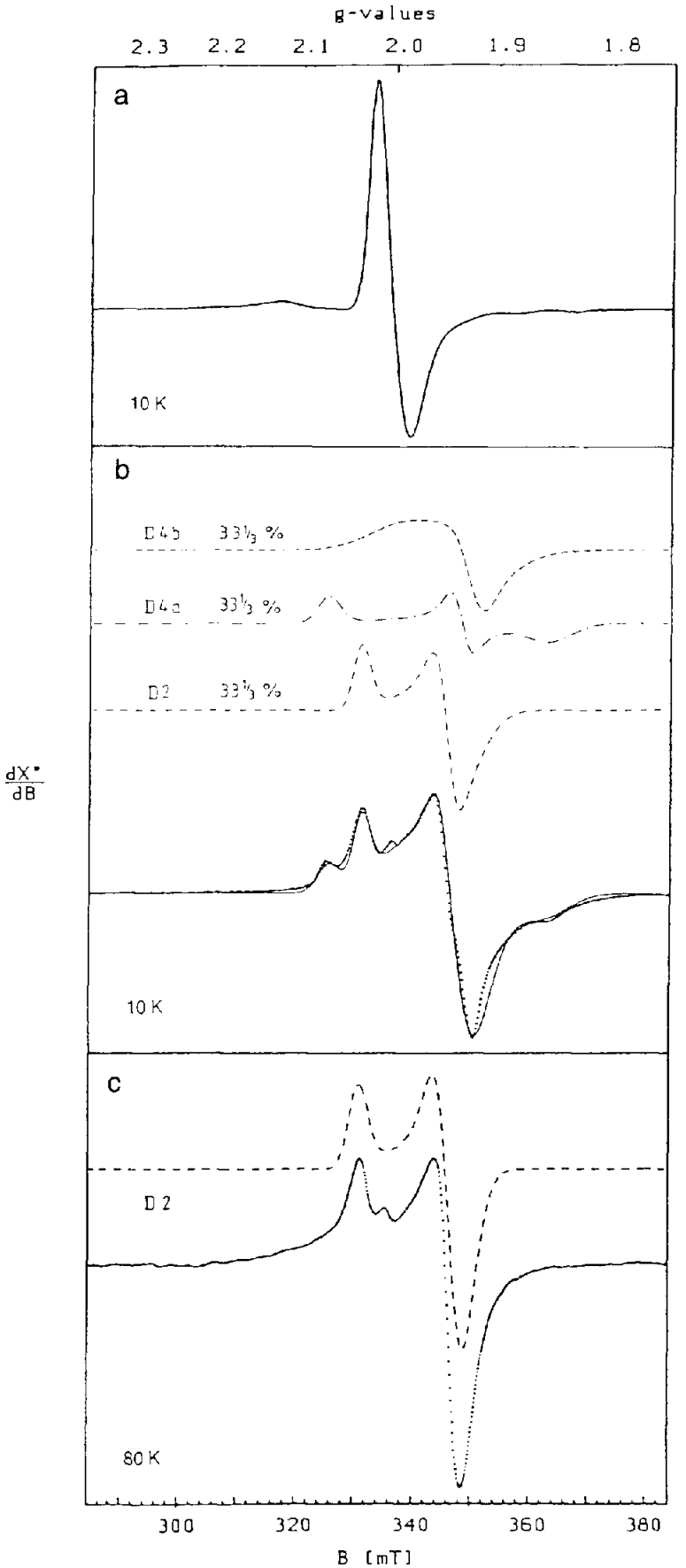

Figure 6. Experimental and simulated EPR spectra of $\alpha\gamma$-dimer preparations. (**a**) Oxidized $\alpha\gamma$-dimer (21 mg/ml), recorded at 10 K, modulation amplitude 1 mT, microwave power 20 μW, frequency 9.415 GHz. (**b**) Reduced with 3 mM dithionite, recorded at 10 K, modulation amplitude 1 mT, microwave power 20 μW, frequency 9.437 GHz. —, superposition of simulated subspectra D2, D4a and D4b with relative intensities as indicated. D2: g = 2.036, 1.947, 1.928 and Γ = 2.3, 2.5, 6.0 mT; D4a: g = 2.073, 1.935, 1.854 and Γ = 3.1, 2.5, 5.8 mT; D4b: g = 2.001, 1.927, 1.921 and Γ = 9.3, 3.2, 9.8 mT. (**c**) Reduced sample recorded at 80 K, microwave power 200 mW, otherwise conditions are as in (**b**). – – – Simulation of D2 as in (**b**).

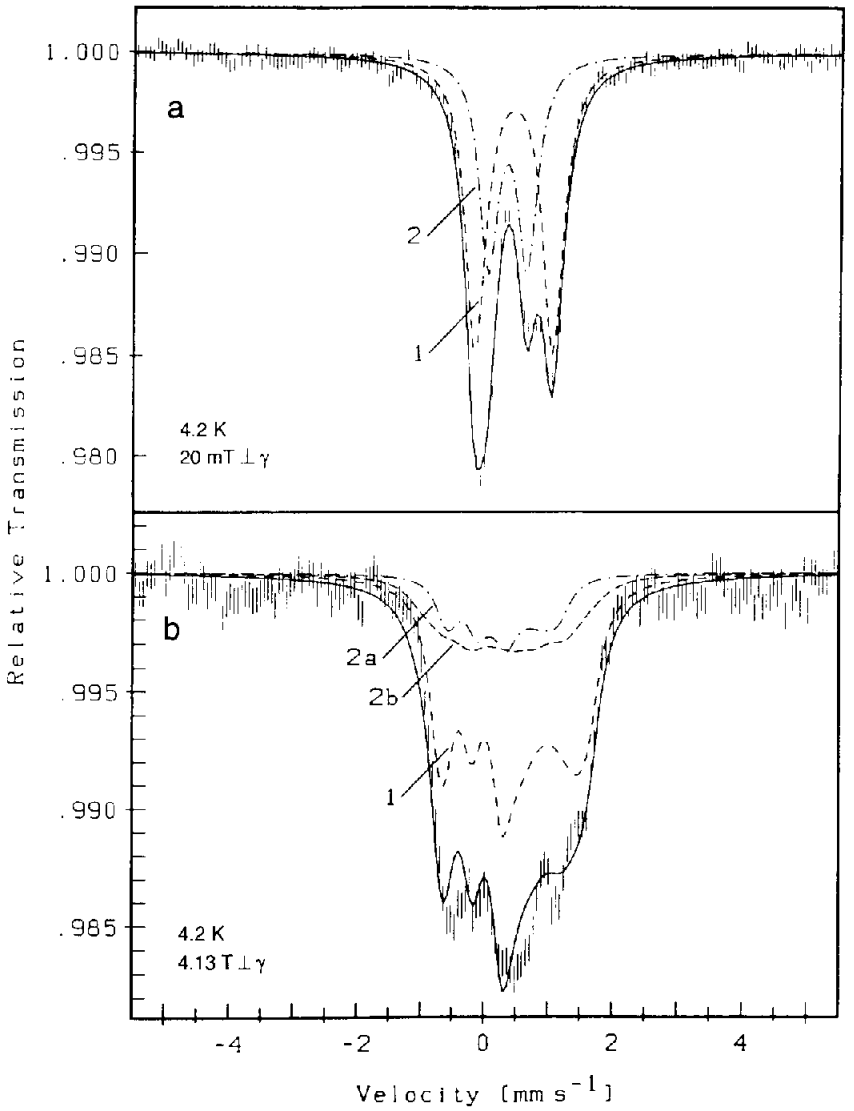

Figure 7. Mössbauer spectra of the oxidized $\alpha\gamma$-dimer, recorded at 4.2 K in a field of (**a**) 20 mT and (**b**) 4.13 T, applied perpendicular to the γ-ray. The subspectra in (**a**) are fits with Lorentzians yielding for subspectrum 1 $\delta = 0.45$ mm/s, $\Delta E_Q = +1.21$ mm/s, $\eta = 0$, $\Gamma = 0.40$ mm/s, and for subspectrum 2 $\delta = 0.35$ mm/s, $\Delta E_Q = +0.61$ mm/s, $\eta = 0$, $\Gamma = 0.37$ mm/s. Subspectra 1 and 2a in (**b**) are simulations for diamagnetic material using the parameters from (**a**); additionally, subspectrum 2b represents the spin-Hamiltonian simulation in fast-relaxation limit with $\delta = 0.33$ mm/s, and $\Delta E_Q = 0.70$ mm/s for the three iron sites ($S = 5/2$) in a $[3Fe\text{-}4S]^{1+}$ cluster. The components of the magnetic hyperfine tensors $A_{xx}/g_n\beta_n$, $A_{yy}/g_n\beta_n$, $A_{zz}/g_n\beta_n$ are $(-34, -28, -32)$ T for site 1, (10, 11, 11) T for site 2 and (2.5, 2.5, 2.5) T for site 3.

10 K (Figure 8b, dotted line). The solid line in Figure 8b is a 1:3 superposition of the corresponding experimental EPR spectra of the $\beta\delta$-dimer and the $\alpha\gamma$-dimer in the reduced state, as depicted in Figures 3b and 6b, respectively. (The 1:3 superposition is due to the presence of one EPR-visible $[4Fe\text{-}4S]^{1+}$ cluster in the $\beta\delta$-dimer, two EPR-visible $[4Fe\text{-}4S]^{1+}$ clusters, one EPR-silent $[3Fe\text{-}4S]^{0}$ cluster and one EPR-visible $[2Fe\text{-}2S]^{1+}$ cluster in the $\alpha\gamma$-dimer.) This superposition shows approximately the same features as the experimental spectrum of the native tetramer. In detail, however, there are deviations, for instance at $g \approx 1.95$ and at $g \approx 2.07$, and particularly, it appears that the spectrum of the native tetramer exhibits less rhombic splitting than the two dimers. We therefore tried to analyse the spectrum of the tetramer further on the basis of the simulated subspectra D2, D4a, D4b and H1, H2 of the individual dimers, and we used the saturation behaviour (at 10 K with 20 μW and 20 mW, respectively) and the temperature dependence (between 10 K and 80 K) for assignments of the overlapping subspectra. [In the following, prime symbols (′) refer to subspectra of the native tetramer.] The trough at $g \approx 1.87$ is part of a component H1′ (Figure 8c) which corresponds to H1 of the isolated $\beta\delta$-dimer in Figure 3, representing $[4Fe\text{-}4S]^{1+}$ clusters. Saturation experiments revealed the complete absence of the component H2′, which corresponds to H2 and which was also assigned to $[4Fe\text{-}4S]^{1+}$ clusters in the isolated $\beta\delta$-dimer. A measurement, recorded at 80 K (not shown), allowed an unambiguous identification of $[2Fe\text{-}2S]^{1+}$ clusters by subspectrum D2′, corresponding to subspectrum D2 in Figure 6c for the isolated $\alpha\gamma$-dimer. Fitting the identified components H1′ and D2′ to the experimental spectrum of the tetramer (25% for each subspectrum) shows that the remaining part of the spectrum can be simulated by a single subspectrum, D4′, accounting for 50% of the total intensity (Figure 8c). As this component, which represents two $[4Fe\text{-}4S]^{1+}$ clusters, differs (especially in its line width) from the two compo-

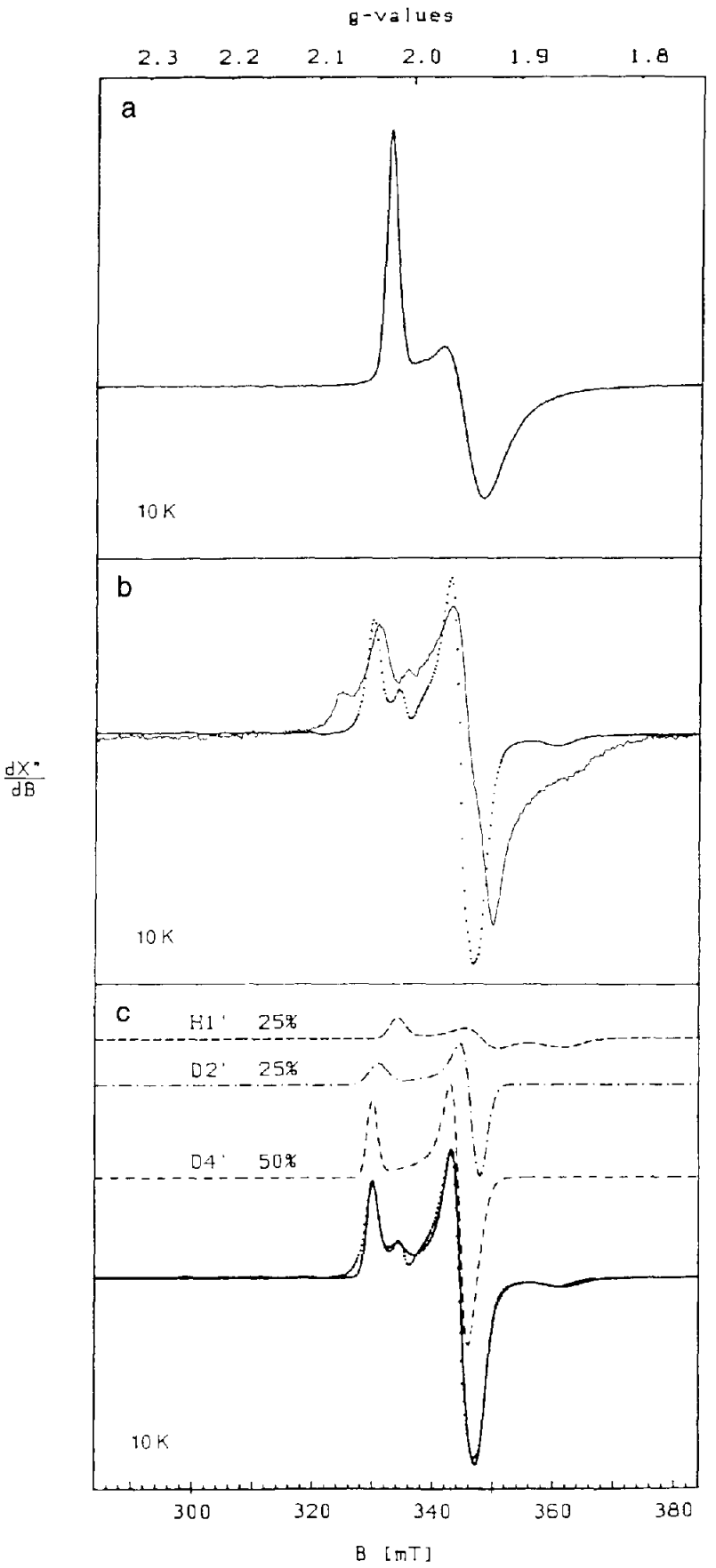

Figure 8. EPR spectra of the native hydrogenase tetramer. (**a**) Oxidized enzyme (24 mg/ml), recorded at 10 K, modulation amplitude 1 mT, microwave power 20 μW, frequency 9.420 GHz. (**b**) Same sample reduced with 3 mM dithionite, recorded at 10 K, modulation amplitude 1 mT, microwave power 20 μW, frequency 9.414 GHz. —, 1:3 superposition of experimental spectra from reduced $\beta\delta$-dimer (Figure 3b) and reduced $\alpha\gamma$-dimer (Figure 6b). (**c**) Same experimental spectrum as (**b**). —, 1 : 1 : 2 superposition of simulated subspectra H1':D2':D4' with H1': g = 2.013, 1.932, 1.858 and Γ = 1.5, 2.5, 3.7 mT; D2': g = 2.034, 1.939, 1.939 and Γ = 1.8, 1.5, 2.0 mT; D4': g = 2.039, 1.952, 1.942 and Γ = 1.0, 1.2, 2.2 mT.

nents D4a and D4b of the isolated $\alpha\gamma$-dimer (compare Figure 6b), we conclude that the $[4Fe\text{-}4S]^{1+}$ clusters undergo conformational changes in the protein moiety when the tetramer is separated into dimers. Thus, the absence of component H2′ in the spectrum of the tetramer and the strong intensity of component H1′, accounting for one $[4Fe\text{-}4S]^{1+}$ cluster in the $\beta\delta$-dimer, corroborates our interpretation from above that H1 and H2 represent two variations of the single [4Fe-4S] cluster in different protein conformations of the isolated $\beta\delta$-dimer.

Discussion

In the present work we have developed a new preparative FPLC procedure to cleave and separate the tetrameric, NAD-linked hydrogenase of *N. opaca* 1b into two distinct heterodimers ($\alpha\gamma$, $\beta\delta$). The high activity yield and the stability of the resulting preparations enabled us to perform a more detailed spectroscopic study on these two protein dimers.

From our analyses of the iron content and of the EPR and Mössbauer spectra, we draw the following conclusions: the $\alpha\gamma$-dimer contains one [3Fe-4S] cluster, which is a natural constituent, one [2Fe-2S] cluster and two [4Fe-4S] clusters; the $\beta\delta$-dimer contains, in addition to nickel, only one [4Fe-4S] center with a midpoint potential of −385 mV; the [3Fe-4S] cluster, present in variable amounts in $\beta\delta$-preparations, was demonstrated to represent an oxidative damage product of the [4Fe-4S] cluster.

These assignments were supported from data of the isolated dimers as well as of the native, tetrameric enzyme. Simulations of the EPR spectra enabled us to monitor changes in cluster geometries during separation of the enzyme into dimers, resulting from alterations of protein conformation. Nearly all clusters experienced such effects on dimer separation. The [4Fe-4S] cluster of the $\beta\delta$-dimer, particularly, exhibited a unique spectrum in preparations of the tetramer, while in isolated dimers two preparation-dependent species were observed. The reason for this behaviour might be that the protein conformation of the $\beta\delta$-dimer is less stable in its isolated form compared to the case when it is embedded in the tetramer. It is tempting to speculate that the sensitivity of the [4Fe-4S] cluster to oxidative degradation into non-physiological [3Fe-4S] clusters might be a further result of this protein instability.

All the current data, taken together with those of a previous study (Schneider *et al.* 1984a,b) allow us to propose the complemented enzyme model shown in Figure 9. The NAD-linked hydrogenase of *N. opaca* is composed of two completely different, individual enzymes: one enzyme is represented by the FMN-containing $\alpha\gamma$-dimer (diaphorase-dimer) and exhibits NADH oxidase activity; the second enzyme is represented by the $\beta\delta$-dimer (hydrogenase-dimer), which behaves like an ordinary hydrogenase catalyzing the H_2 evolution and H_2 uptake with artificial electron carriers. NAD reduction with H_2 is only catalyzed by the whole tetrameric enzyme. This model implies that an intramolecular and subunit-overlapping electron transport has to take place before NAD can be reduced by hydrogen.

[3Fe-4S] clusters have repeatedly been proposed, particularly in connection with aconitase (Beinert *et al.* 1983) and hydrogenases (Cammack *et al.* 1982, Schneider *et al.* 1984b), to have a regulatory function in enzymes. In Ni-containing hydrogenases a [3Fe-4S] cluster may play a role in the reductive activation/oxidative deactivation process as described by Cammack *et al.* (1988). However, we have to consider, firstly, that the [3Fe-4S] cluster detected in the *N. opaca* hydrogenase is not located in the hydrogenase-dimer but in the diaphorase-dimer, and secondly, that [3Fe-4S] clusters generally are not present in all Ni-containing hydrogenases. For example, the hydrogenase of *Desulfovibrio gigas* definitely contains a [3Fe-4S] cluster (Huynh *et al.* 1987), whereas the hydrogenase of *Desulfovibrio baculatus* does not (Teixeira *et al.* 1990). Thus, the existence of a [3Fe-4S] cluster does not

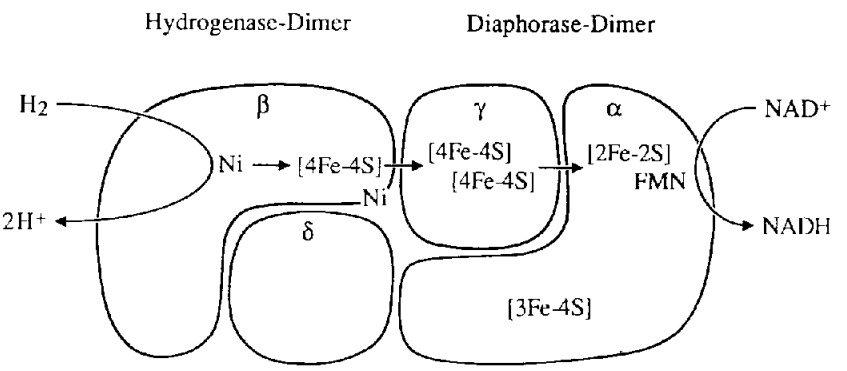

Figure 9. Enzyme model for the structural and functional organization of the cytoplasmic, NAD-reducing hydrogenase of *N. opaca* 1b. The arrangement and shape of the four subunits are based on electron microscopy studies. Physiological direction of enzyme reaction and electron transport is indicated by arrows. The NAD-linked hydrogenase appears to contain two atoms of Ni. One represents the catalytically active Ni center, the second one has been postulated to play a role in the binding of subunits (Schneider *et al.* 1984b). This is indicated by placing the second Ni atom at the 'edge' of the β subunit close to the γ subunit. A definite assignment of the [3Fe-4S] cluster to one certain diaphorase-dimer subunit is not possible. This cluster may be ligated to the α subunit, to the γ subunit, or to both.

appear to be a prerequisite for a reductive activation of hydrogenase or for an active hydrogenase in general. The results and interpretations of the present work are in conflict with the proposal of Tran-Betcke *et al.* (1990) that a [3Fe-4S] cluster is located in the δ subunit of the NAD-reducing hydrogenase from *A. eutrophus* H16. However, no experimental evidence exists for such an assignment: because the *A. eutrophus* hydrogenase does not dissociate into intact heterodimers, it was not possible to study the metal centers of the two dimers separately and to localize a potentially existing [3Fe-4S] cluster.

The most important result of the present study is the conclusive evidence that the hydrogenase($\beta\delta$)-dimer contains the nickel center and only one [4Fe-4S] cluster. These constituents are sufficient to confer the hydrogenase function within the tetrameric enzyme system, i.e. to activate hydrogen and to transfer electrons from hydrogen to the Fe-S clusters of the diaphorase($\alpha\gamma$)-dimer. Hornhardt *et al.* (1986, 1990) succeeded in isolating a native subunit of the hydrogenase from a mutant of *A. eutrophus*, which corresponds to the β subunit of the hydrogenase ($\beta\delta$)-dimer from *N. opaca*. This subunit contained nickel as well as one Fe-S cluster. The Fe-S cluster was not yet identified unambiguously, but, regarding our present knowledge, it must be a low-potential [4Fe-4S] cluster, analogous to that cluster which we have detected in the $\beta\delta$-dimer. From this it consequently follows, that both the Ni-center and the [4Fe-4S] cluster are located in the large subunit (β) of the hydrogenase($\beta\delta$)-dimer.

Based on these results and interpretations, the model for the spatial and functional organization of the NAD-reducing hydrogenase as proposed by Tran-Betcke *et al.* (1990) must be revised. Tran-Betcke and co-workers assume a linear arrangement of the subunits according to the structural model proposed by Tsuprun *et al.* (1986). According to this 'linear model', direct binding of the two dimers only occurs between the two small subunits: therefore, this model allows no other electron transport than that from β (the subunit containing the site for H_2 activation) to δ, then to γ and finally to α (the subunit containing the site for NAD reduction/NADH oxidation). Our conclusion that the δ subunit does not contain any cofactor or metal center and, hence, is not integrated in the intramolecular electron-transfer system, contradicts this linear model, but it is in conformity with the structural model recently deduced by Johannssen *et al.* (1991) from their electronmicroscopy studies. Johannssen and colleagues described a compact subunit system composed of L-shaped large subunits (α, β) and spherical to square-shaped small subunits (γ, δ). There is a close attachment between α and γ and between β and δ, as well as between α and δ and between β and γ, whereas the contact region between the two small subunits appears to be comparatively small in this model. This 'compact model' which was confirmed for both, NAD-reducing hydrogenase of *A. eutrophus* H16 as well as of *N. opaca* 1b (Johannssen *et al.* 1991), implies an electron flow directly from β to γ and then to α, in accordance with our concept (Figure 9). The presence of the two low-potential [4Fe-4S] clusters in the γ subunit has been indicated by a characteristic sequence of eight cysteine residues (Tran-Betcke *et al.* 1990). The location of the NAD(H) reaction site and, as we speculate, also of FMN and the [2Fe-2S] cluster in the α subunit was demonstrated by the capability of this subunit to have still NADH-oxidizing activity after separation of the γ subunit (Hornhardt *et al.* 1990).

It should be finally noted that the diaphorase-dimer which was shown to have NADH : acceptor oxidoreductase activity, exhibits pronounced sequence homologies with subunits of the mitochondrial NADH-ubiquinone reductase complex I from cattle (Pilkington *et al.* 1991) and *Neurospora crassa* (Preis *et al.* 1991).

Acknowledgments

This work was supported by grants from the Deutsche Forschungsgemeinschaft. We gratefully acknowledge the co-operation of Dr R. Brinkmann (Göttingen) in providing cells of *N. opaca* 1b and of Professor Dr A. Müller and C. Hess-Riechmann (Bielefeld) for permission to perform the metal analyses, respectively.

References

Aasa R, Vänngård T. 1975 EPR signal intensity and powder shapes: a reexamination. *J Magn Res* **19**, 308–315.

Adams MWW, Mortenson LE. 1984 The physical and catalytic properties of hydrogenase II of *Clostridium pasteurianum*. *J Biol Chem* **259**, 7045–7055.

Aggag M, Schlegel HG. 1974 Studies on a gram-positive hydrogen bacterium *Nocardia opaca* 1b III. Purification, stability and some properties of the soluble hydrogen dehydrogenase. *Arch Microbiol* **100**, 25–29.

Beinert H, Emptage MH, Dreyer J-L *et al.* 1983 Iron-sulfur stoichiometry and structure of iron-sulfur clusters in three-iron proteins: evidence for [3Fe-4S] clusters. *Proc Natl Acad Sci USA* **80**, 393–396.

Beisenherz G, Bolze HJ, Bücher T *et al.* 1953 Diphosphofructose-Aldolase, Phosphoglyceraldehyd-Dehydrogenase, Milchsäure-Dehydrogenase, Glycerophosphat-Dehydrogenase und Pyruvat-Kinase aus Kaninchenmuskulatur in einem Arbeitsgang. *Z Naturforsch* **8b**, 555–577.

Cammack R, Lalla-Maharajh WV, Schneider K. 1982 EPR-studies of some oxygen-stable hydrogenases. In: Ho C, ed. *Electron Transport and Oxygen Utilization*. New York: Elsevier/North Holland; 411–415.

Cammack R, Fernandez VM, Schneider K. 1988 Nickel in hydrogenases from sulfate-reducing, photosynthetic, and hydrogen-oxidizing bacteria. In: Lancaster JR, ed. *The Bioinorganic Chemistry of Nickel*. New York: VCH Verlagsgesellschaft; 167–190.

Dunham WR, Bearden AJ, Salmeen IT *et al.* 1971 The two-iron ferredoxins in spinach, parsley, pigadrenal cortex, *Azotobacter vinelandii*, and *Clostridium pasteurianum*: studies by magnetic field Mössbauer spectroscopy. *Biochim Biophys Acta* **253**, 134–152.

Dutton PL. 1978 Redox potentiometry: determination of midpoint potentials of oxidation-reduction components of biological electron-transfer systems. *Meth Enzymol* **54**, 411–435.

Emptage MH, Kent TA, Huynh BH, Rawlings J, Orme-Johnson WH, Münck E. 1980 On the nature of the iron-sulfur centers in a ferredoxin from *Azotobacter vinelandii*. *J Biol Chem* **255**, 1793–1796.

Grande HJ, Dunham WR, Averill B, Van Dijk C, Sands RH. 1983 Electron paramagnetic resonance and other properties of hydrogenases isolated from *Desulfovibrio vulgaris* (strain Hildenborough) and *Megasphaera elsdenii*. *Eur J Biochem* **136**, 201–207.

Hornhardt S, Schneider K, Schlegel HG. 1986 Characterization of a native subunit of the NAD-linked hydrogenase isolated from a mutant of *Alcaligenes eutrophus* H16. *Biochimie* **68**, 15–24.

Hornhardt S, Schneider K, Friedrich B, Vogt B, Schlegel HG, 1990 Identification of distinct NAD-linked hydrogenase protein species in mutants and nickel-deficient wild-type cells of *Alcaligenes eutrophus* H16. *Eur J Biochem* **189**, 529–537.

Huynh BH, Czechowski MH, Krüger H-J, DerVartanian DV, Peck HD, Jr, Le Gall J. 1984 *Desulfovibrio vulgaris* hydrogenase: a non heme iron enzyme lacking nickel that exhibits anomalous EPR and Mössbauer spectra. *Proc Natl Acad Sci USA* **81**, 3728–3732.

Huynh BH, Patil DS, Moura I *et al.* 1987 On the active sites of the [NiFe] hydrogenase from *Desulfovibrio gigas*. Mössbauer and redox-titration studies. *J Biol Chem* **262**, 795–800.

Johannssen W, Gerberding H, Rohde M, Zaborosch C, Mayer F. 1991 Structural aspects of the soluble NAD-dependent hydrogenase isolated from *Alcaligenes eutrophus* and from *Nocardia opaca* 1b. *Arch Microbiol* **155**, 303–308.

Lorenz B, Schneider K, Kratzin H, Schlegel HG. 1989 Immunological comparison of subunits isolated from various hydrogenases of aerobic hydrogen bacteria. *Biochim Biophys Acta* **995**, 1–9.

Middleton P, Dickson DPE, Johnson CE, Rush JD. 1980 Interpretation of the Mössbauer spectra of the high-potential iron protein from *Chromatium*. *Eur J Biochem* **104**, 289–296.

More KM, Eaton GR, Eaton SS. 1986 Metal nitroxyl interactions. 47. EPR spectra of two spin-labeled derivatives of EDTA coordinated to paramagnetic metal ions. *Inorg Chem* **25**, 2638–2646.

Moura JJG, Moura I, Kent TA *et al.* 1982 Interconversions of [3Fe-3S] and [4Fe-4S] clusters *J Biol Chem* **257**, 6259–6267.

Moura JJG, LeGall J, Xavier AV. 1984 Interconversion from 3Fe into 4Fe clusters in the presence of *Desulfovibrio gigas* cell extracts. *Eur J Biochem* **141**, 319–322.

Münck E. 1982 Mössbauer studies of [3Fe-3S] clusters and sulfide reductase. In: Spiro TG, ed. *Iron Sulfur Proteins*. New York: Wiley; 147–175.

Orme-Johnson WH, Orme-Johnson NR. 1982 Iron-sulfur proteins: the problem of determining cluster type. In: Spiro TG, ed. *Iron Sulfur Proteins*. New York: Wiley; 67–96.

Pilkington SJ, Skehel JM, Gennis RB, Walker JE. 1991 Relationship between mitochondrial NADH ubiquinone reductase and a bacterial NAD-reducing hydrogenase. *Biochemistry* **30**, 2166–2175.

Preis D, Weidner U, Conzen C *et al.* 1991 Primary structures of two subunits of NADH-ubiquinone reductase from *Neurospora crassa* concerned with NADH oxidation. Relationship to a soluble NAD-reducing hydrogenase of *Alcaligenes eutrophus*. *Biochim Biophys Acta* **1090**, 133–138.

Rupp H, Rao KK, Hall DO, Cammack R. 1978 Electron spin relaxation of iron-sulphur proteins studied by microwave power saturation. *Biochim Biophys Acta* **537**, 255–269.

Schlegel HG, Kaltwasser H, Gottschalk G. 1961 Ein Submersverfahren zur Kultur wasserstoffoxidierender Bakterien: Wachstumsphysiologische Untersuchungen. *Arch Mikrobiol.* **38**, 209–222.

Schneider K, Piechulla B. 1986 Isolation and immunological characterization of the four non-identical subunits of the soluble, NAD-linked hydrogenase from *Alcaligenes eutrophus* H16. *Biochimie* **68**, 5–13.

Schneider K, Schlegel HG. 1976 Purification and properties of soluble hydrogenase from *Alcaligenes eutrophus* H16. *Biochim Biophys Acta* **452**, 66–80.

Schneider K, Cammack R, Schlegel HG, Hall DO. 1979 The iron-sulphur centres of soluble hydrogenase from *Alcaligenes eutrophus*. *Biochim Biophys Acta* **578**, 445–461.

Schneider K, Schlegel HG, Jochim K. 1984a Effect of nickel on activity and subunit composition of purified hydrogenase from *Nocardia opaca* 1b. *Eur J Biochem* **138**, 533–541.

Schneider K, Cammack R, Schlegel HG. 1984b Content and localization of FMN, Fe-S clusters and nickel in the NAD-linked hydrogenase of *Nocardia opaca* 1b. *Eur J Biochem* **142**, 75–84.

Slappendel S, Veldink GA, Vliegenhart JFG, Aasa R, Malmström BG. 1980 EPR spectroscopy of soybean lipoxygenase-1: determination of the zero-field splitting constants of high-spin Fe(III) signals from temperature and microwave frequency dependence. *Biochim Biophys Acta* **624**, 30–39.

Teixeira M, Fauque G, Moura I *et al.* 1987 Nickel-[iron-sulfur]-selenium-containing hydrogenase from *Desulfovibrio baculatus* (DSM 1743). *Eur J Biochem* **167**, 47–58.

Teixeira M, Moura I, Xavier AV *et al.* 1989 Redox intermediates of *Desulfovibrio gigas* [NiFe] hydrogenase generated under hydrogen: Mössbauer and EPR characterization of the metal centers. *J Biol Chem* **264**, 16435–16450.

Teixeira M, Moura I, Fauque G *et al.* 1990 The iron-sulfur centers of the soluble [NiFeSe] hydrogenase from *Desulfovibrio baculatus* (DSM 1743)-EPR and Mössbauer characterization. *Eur J Biochem* **189**, 381–386.

Thomsom AJ, Robison AE, Johnson MK *et al.* 1981 Low-temperature magnetic circular dichroism evidence for the conversion of four-iron-sulphur clusters in a ferredoxin from *Clostridium pasteurianum* into three-iron-sulphur clusters. *Biochim Biophys Acta* **670**, 93–100.

Tran-Betcke A, Warnecke U, Böcker C, Zaborosch C, Friedrich B. 1990 Cloning and nucleotide sequences of the genes for the subunits of NAD-reducing hydrogenase of *Alcaligenes eutrophus* H16. *J Bacteriol* **172**, 2920–2929.

Trautwein AX, Bill E, Bominaar EL, Winkler H. 1991 Iron-containing proteins and related analogs—complementary Mössbauer, EPR and magnetic susceptibility studies. *Structure and Bonding* **78**, 1–96.

Tsuprun VL, Utkin IB, Popov VO, Egorov AM, Berezin IV, Kiselev NA. 1986 Electron microscopy of the hydrogenase from the hydrogen-oxidizing bacterium *Alcaligenes eutrophus* Z1. *FEBS Lett* **197**, 225–228.

Twilfer H, Gersonde K, Christahl M. 1981 Resolution enhancement of EPR spectra using the Fourier transform technique. Analysis of nitrosyl cytochrome c oxidase in frozen solution. *J Magn Res* **44**, 470–478.

Vanhoe H, Vandecasteele C, Versiek J, Dams R. 1989 Determination of iron, cobalt, copper, zinc, rubidium, molybdenum, and cesium in human serum by inductively coupled plasma mass spectrometry. *Anal Chem* **61**, 1851–1857.

Zaborosch C, Schneider K, Schlegel HG, Kratzin H. 1989 Comparison of the NH_2-terminal amino acid sequences of the four non-identical subunits of the NAD-linked hydrogenases from *Nocardia opaca* 1b and *Alcaligenes eutrophus* H16. *Eur J Biochem* **181**, 175–180.